Available online at www.sciencedirect.com

SciVerse ScienceDirect

Ceramics International 39 (2013) 5165–5174

CERAMICS INTERNATIONAL

www.elsevier.com/locate/ceramint

Phase transformation and nanocrystallite growth behavior of 2 mol% yttria-partially stabilized zirconia (2Y-PSZ) powders

Chau-Hsiang Wang[a,b], Moo-Chin Wang[c,*], Je-Kang Du[a,b], Yu-You Sie[a], Chi-Shiung Hsi[d], Huey-Er Lee[a,b,**]

[a]*Department of Dentistry, Kaohsiung Medical University, 100 Shih-Chuan 1st Road, Kaohsiung 807, Taiwan*
[b]*Department of Dentistry, Kaohsiung Medical University, Chung Ho Memorial Hospital, 100 Tzyou 1st Road, Kaohsiung 807, Taiwan*
[c]*Department of Fragrance and Cosmetic Science, Kaohsiung Medical University, 100 Shih-Chuan 1st Road, Kaohsiung 807, Taiwan*
[d]*Department of Materials Science and Engineering, National United University, 1 Lein-Da, Kung-Ching Li, Miao-Li 36003, Taiwan*

Received 29 September 2012; received in revised form 4 December 2012; accepted 5 December 2012
Available online 20 December 2012

Abstract

Two mol% yttria-partially stabilized zirconia (2Y-PSZ) precursor powders were obtained through a co-precipitation process using $ZrOCl_2.8H_2O$ and $Y(NO_3)_3.6H_2O$ as starting materials. Phase transformation and crystallite growth behavior have been investigated using X-ray diffraction (XRD), transmission electron microscopy (TEM) and selected area electron diffraction (SAED). XRD results show that the crystal structure to be composed of coexisting tetragonal ZrO_2 (t-ZrO_2) and monoclinic ZrO_2 (m-ZrO_2) when the 2Y-PSZ freeze dried precursor powders was calcined at 773–1273 K for 2 h. The fraction of m-ZrO_2 content is lower than 3.0 % when the calcination temperature is lower than 1073 K, whereas m-ZrO_2 content rapidly increases to 8.7 % with the increase of calcination temperature to 1273 K. The crystallite size of t-ZrO_2 increases from 12.3 to 30.2 nm when calcination temperature increased from 773 to 1273 K. In addition, the activation energy of t-ZrO_2 and m-ZrO_2 crytallite growth in 2Y-PSZ freeze dried precursor powders are 29.2 and 21.8 kJ/mol, respectively.

Keywords: Phase transformation; Yttria-partial stabilized zirconia; Tetragonal ZrO_2; Activation energy

1. Introduction

In 1999, Piconi and Maccauro [1] pointed out that yttria-stabilized tetragonal zirconia (Y-TZP) has become increasingly popular as an alternative high-toughness core material in dental restorations because of its biocompatibility, attractive mechanical properties and superior natural appearance compared with metal dental restorations. The replacement of traditional metal-based fixed partial dentures with all-ceramic prosthetic crowns and bridges has been driven by the improved aesthetics and excellent tissue compatibility achieved using tooth-colored, metal-free system have been reported by Kelly [2]. From the same reasons, the traditionally used metal and alloys can be replaced by zirconia (ZrO_2) full-ceramic post and core systems, implant suprastractures, root dental posts, crowns and fixed partial dentures [3–6].

ZrO_2 is a polymorphic material that exists in three allotropes i.e. cubic (c), tetragonal (t), and monoclinic (m) symmetry and stable at high (2953–2643 K), intermediate (2643–1223 K), and low (below 1223 K) temperatures [7]. The pure ZrO_2 ceramics used as advanced structure materials is limited by the spontaneous stress-induced martensitic transformation from t→m when from

*Corresponding author. Tel.: +886 7 3121101x2366; fax: +886 7 3210683.
**Corresponding author. Tel: +886 7 3121101x7003; fax: +886 7 3318029.
E-mail addresses: mcwang@kmu.edu.tw (M.-C. Wang), huerle@kmu.edu.tw (H.-E. Lee).

0272-8842/$ - see front matter
http://dx.doi.org/10.1016/j.ceramint.2012.12.013

elaboration temperature to room temperature. To avoid phase transformation through the heating and cooling cycles, the 8 mol% Y_2O_3 stabilized zirconia (YSZ) ceramics with a single cubic phase was desirable for high temperature application as proposed by Pascual and Duran [8]. When added 3–5 mol% Y_2O_3 to ZrO_2, fine-grain t-ZrO_2 polycrystals (Y-TZP) and partially stabilized ZrO_2 (Y-PSZ) have excellent strength and fracture toughness due to the stress-induced martensitic transformation from t→m occurred [9].

Three types of ZrO_2 ceramics are available for dental application, namely 3 mol% Y_2O_3-tetragonal ZrO_2 polycrystals (3Y-TZP), ZrO_2-toughened alumina (ZTA) and magnesium partially stability ZrO_2 (Mg-PSZ) [1]. The phenomenon of ZTA due to the stress-induced martensitic transformation from t-ZrO_2 to m-ZrO_2 is combined with alumina (Al_2O_3) matrix [10,11]. These materials possess interest for potential use as bioceramic [12].

As mentioned above, the retention of the tetragonal phase (t-phase) to monoclinic phase (m-phase) at room temperature is essential to increase the fracture strength and fracture toughness of TZP. Due to high strength and toughness when compared with other ceramics, TZP has been regarded as an important biomedical ceramic. Various processes to synthesize the TZP powders and discussion on the properties in detailed have been reported by several researchers [13–19]. Structural and textural studies on ZrO_2–Y_2O_3 samples prepared by heat treating microporous gels in air or under vacuum have been reported by Álvarez et al. [13]. Zhu and Yan [14] discussed the relationship between grain size and the kinetics of t→m isothermal transformation for 2 mol% Y_2O_3–ZrO_2 ceramics prepared by the co-precipitation technique. Wu et al. [15] pointed out that using a precipitation process with hexamethyldisilazane vapor treatment the synthesized nanocrystallites tetragonal ZrO_2 (t-ZrO_2) can be enhanced the stability of t-phase. Moreover, Vasylkiv and Sakka [16] also demonstrated that nanosized 3Y-TZP powders can be obtained by hydrothermal precipitation from metal zirconium chloride and urea sol using a washing–drying treatment and calcination. Li and Guo [17,18] proposed the synthesis of 3Y-TZP powders by heating ethanol-agueous salt solutions and reported their compacting and sintering behavior. Viazzi et al. [19] reported the formation of metastable t-phase (t') after calcinations in the temperature range of 1373–1673 K, which was produced via a sol–gel route using $Zr(OPr)_4$ and $Y(NO_3)_3$ as starting materials.

The nanocrystallite powders of 3 mol% yttria-partially stabilized zirconia (3Y-PSZ) have been obtained using $ZrOCl_2$ and $Y(NO_3)_3$ as the raw materials with a co-precipitation process in an alcohol–water solution. The activation energy of 401.89 kJ/mol was obtained when the t→m transformation occurred in the 3Y-PSZ freeze dried precursor powders [20]. Moreover, Hsu et al. [21] also pointed out that using a non-isothermal method, the activation energy of 169.2 ± 21.9 kJ/mol was obtained for the tetragonal ZrO_2 crystallization from 3 mol% yttria stabilized tetragonal zirconia freeze dried precursor powders. However, an extensive literature search showed that the phase transformation and nanocrystallite growth behavior of the 2 mol% yttria-partially stability zirconia (2Y-PSZ) powders prepared at pH 7 using a co-precipitation process have not been studied in detail.

In the present study, high purity of zirconium oxychloride ($ZrOCl_2 \cdot 8H_2O$) and yttrium nitrate ($Y(NO_3)_3 \cdot 6H_2O$) have been used as starting materials for synthesis of 2Y-PSZ nanocrystallite powders via a co-precipitation process. X-ray diffraction (XRD), Brunauer–Emmett–Teller (BET) isotherm, transmission electron microscopy (TEM) and select area electron diffraction (SAED) have been utilized to characterize the phase transformation and crystallite growth of 2Y-PSZ precursor powders prepared at pH 7. The purposes of this investigated were (i) to study the phase transformation behavior for the 2Y-PSZ freeze dried precursor powders after calcined at various temperatures, (ii) to evaluate the kinetics of crystallite growth of t-ZrO_2 and m-ZrO_2, and (iii) to observe the microstructure for the 2Y-PSZ freeze dried precursor powders calcined at various temperatures.

2. Experimental procedure

2.1. Sample preparation

The zirconium oxychloride ($ZrOCl_2 \cdot 8H_2O$, purity≧ 99.5%, supplied by Riedel-de Haën, Germany) and yttrium nitrate ($Y(NO_3)_3 \cdot 6H_2O$, supplied by Acros, New Jersey, USA) used as the starting materials and dissolved in a solution of deionized water mixed with ethanol in a volume ratio of 1:5. A molar ratio of Y_2O_3 to ($Y_2O_3 + ZrO_2$) was fixed at 0.02 and labeled as 2Y-PSZ. Then, the mixture solution was added with certain amount of polyethylenglycol (PEG, extra pure reagent, molecular weight 2000 Da, supplied by Nippon Shiyaku Kogyo K. K., Japan) as a dispersant. The mixture solution was stirred and heated to 348 K in a thermostatic bath to obtain white gel-like precipitates. Ammonium hydroxide (NH_4OH, purity 28%, supplied by Nihon Shiyaku Reagent, Japan) was then added into the gel controlled pH at 7. After precipitation, the gel was repeatedly rinsed with a large amount of deionized water and tested with $AgNO_3$ solution to make sure no AgCl precipitation had occurred, and then the precipitutes were freeze-dried at 218 K in vacuum. Samples calcining were carried in air using a mullite circle. Powders were cooling in air and each sample was characterized by XRD.

2.2. Sample characterization

The crystalline phase of 2Y-PSZ freeze dried precursor powders after calcination was identified by XRD (Rigaku, D-Max/IIIV, Tokyo, Japan), with a monochromatic CuKα radiation ($\lambda = 0.1540$ nm) and Ni filter. The operation voltage and current were 30 kV and 20 mA, respectively, at a scanning rate of 0.25°/min.

The average crystalline size of the t-, or m- ZrO_2 of the 2Y-PSZ precursor powders prepared at pH 7 and calcined at various temperatures for 2 h are calculated by the Scherrers equation as follows [22]:

$$D_{hkl} = 0.89\lambda/\beta\cos\theta \quad (1)$$

where D_{hkl} is the average crystallite size of the t- and m- ZrO_2 of the 2Y –PSZ freeze dried precursor powders after calcination, $\lambda = 0.1540$ nm is the X-ray wavelength of CuKα, β denotes the full width of the peak measured at half maximum intensity (FWHM) of t- and m-ZrO_2, and θ is the Bragg's angle of the reflection peak of maximum density of t- and m-ZrO_2, respectively.

The volume fractions of the m-ZrO_2 (m%) and t-ZrO_2 (t%) phases are calculated using the following formula suggested by Garvie and Nicholson [23]:

$$[m\,\% = I_m(\bar{1}11) + I_m(111)]/[I_m(\bar{1}11) + I_t(101) + I_m(111)] \quad (2)$$

$$t\,\% = I_t(101)/[I_m(\bar{1}11) + I_t(101) + I_m(111)] \quad (3)$$

where $I_m(\bar{1}11)$ and $I_m(111)$ refers to the relative integrated area under the $(\bar{1}11)$ and (111) reflection peaks of the m-ZrO_2 phase and $I_t(101)$ refers to the relative integrated area under the (101) reflection peak of the t-ZrO_2 phase.

The specific surface area of the resulting powders was measured by Brunauer–Emmett–Teller (BET) technique using nitrogen as an adsorption. The measured surface area was converted to the equivalent particle size using the following equation [24]:

$$d_{BET} = \frac{\kappa}{\rho s_{BET}} \quad (4)$$

where d_{BET} is the average particle size, κ is the shape coefficient (close to a spherical shape, $\kappa = 6$), S_{BET} is the specific surface are expressed in m^2/g, and $\rho = 6$ is the theoretical density of the yttria-stabilized zirconia (YSZ) in g/cm^3.

The morphology and crystal structure of the post-calcined powders were determined by a TEM (Hitachi FE-2000, Tokyo, Japan) operated at 200 kV. The crystal structure of the 2Y-PSZ powders was determined by SAED. The TEM sample was prepared by dispersing the 2Y-PSZ powders in an ultrasonic bath and then collected in a copper grid.

3. Results

3.1. Phase transformation and crystal structure of the 2 Y-PSZ freeze dried precursor powders after calcination

The X-ray diffraction (XRD) patterns of the 2Y-PSZ freeze dried precursor powders prepared at pH 7 and calcined at 773 K to 873 K for 2 h are shown in Figs. 1 and 2, respectively. Fig. 1(a) shows that the characteristic (004) reflection peak of t-ZrO_2 phase did not appear, but the (2 2 0) reflection peak of t-ZrO_2 appeared. On the other hand, the $(\bar{1}11)$ reflection peak of m-ZrO_2 phase also accompany

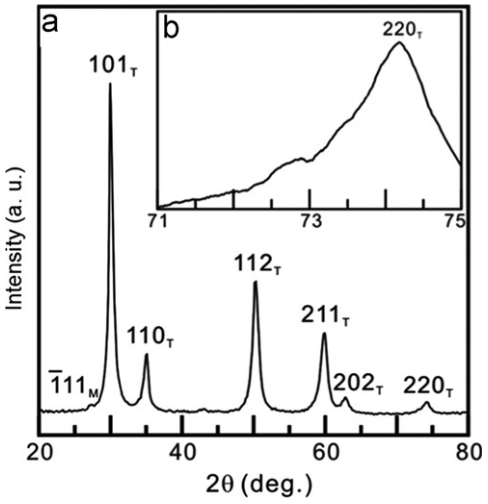

Fig. 1. (a) XRD pattern of 2Y-PSZ freeze dried precursor powders calcined at 773 K for 2 h and (b) zoom on the 70–75° (2θ) area.

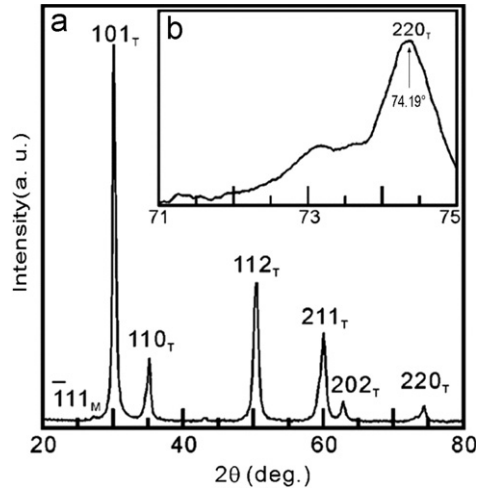

Fig. 2. (a) XRD pattern of 2Y-PSZ freeze dried precursor powders calcined at 873 K for 2 h and (b) zoom on the 70–75° (2θ) area.

appeared but lower intensity. Fig. 1(b) shows the enlarged view of the Bragg's angle (2θ) from 70 to 75° which reveals that (220) reflection peak of t-ZrO_2 appeared at 74.19°. According to the results of Fig. 1(a) and (b) which indicated that the phases of 2Y-PSZ freeze dried precursor powders calcined at 773 K for 2 h contains the t-ZrO_2 and m-ZrO_2 as the predominant and minor phases, respectively. When the 2Y-PSZ freeze dried precursor powders calcined at 873 K for 2 h, which XRD patterns under the detection level and the enlarged view of 2θ from 70 to 75° are shown in Fig. 2(a) and (b), respectively. From Fig. 2(a), it is seen that the t-ZrO_2 was still maintained the predominant phase, and the m-ZrO_2 also as the minor phase, respectively. Further, the result of Fig. 2(b) is similar to the Fig. 1(b), only the (220) reflection peak of t-ZrO_2 appeared.

Although the (200) and (004) reflection peaks of t-ZrO_2 almost could not be observed in Figs. 1 and 2. However, this result does not affect the calculated volume fraction of

m-ZrO_2 and t-ZrO_2 due to the Eqs. (2) and (3) are not use the I_t (200) and I_t (004). Therefore, the volume fraction of m-ZrO_2 and t-ZrO_2 in the present study are reliable.

When the 2Y-PSZ freeze dried precursor powders calcined at 1073 K for 2 h which XRD patterns under the detection level and the enlarged view of 2θ from 70 to 75° are shown in Fig. 3(a) and (b), respectively. The result of Fig. 3(a) reveals the $(110)_t$ reflection split into $(002)_t$ and $(110)_t$, and $(211)_t$ reflection split into $(103)_t$ and $(211)_t$, respectively, due to the characteristic t-ZrO_2 phase. From Fig. 3(b), the characteristic $(400)_t$ reflection peak of c-ZrO_2 (2θ around 73.94°) was no more observed, but the characteristic $(004)_t$ peak of the t-ZrO_2 appeared.

Fig. 4(a) and (b) show the XRD patterns of the detection level and enlarged view of 2θ from 70 to 75°, respectively, for 2Y-PSZ freeze dried precursor powders calcined at 1273 K. It is seen that the results of Fig. 4(a) and (b) are similar to that of Fig. 3(a) and (b), except that the $(110)_t$ reflection split into $(002)_t$ and $(110)_t$, $(211)_t$ reflection split into $(103)_t$ and $(211)_t$, and $(200)_t$ reflection first appeared from $(112)_t$ reflection and began to split in Fig. 4(a).

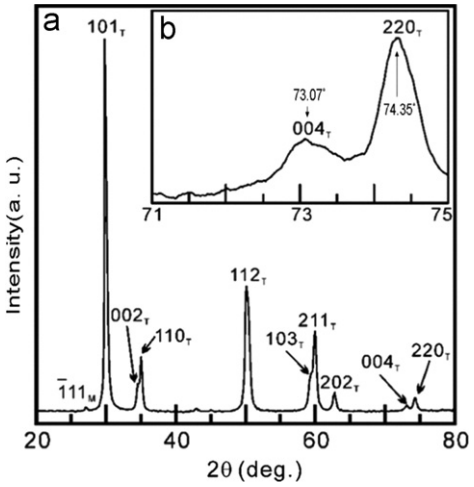

Fig. 3. (a) XRD pattern of 2Y-PSZ freeze dried precursor powders calcined at 1073 K for 2 h and (b) zoom on the 70–75° (2θ) area.

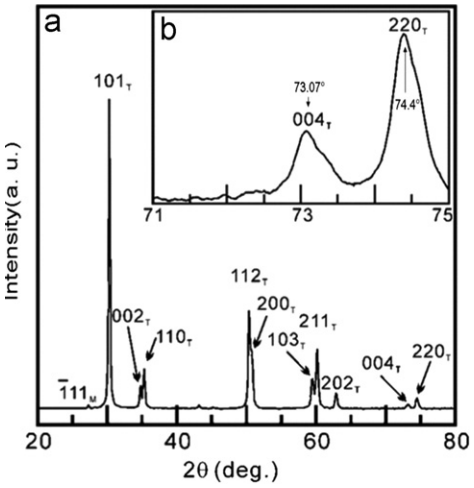

Fig. 4. (a) XRD pattern of 2Y-PSZ freeze dried precursor powders calcined at 1273 K for 2 h and (b) zoom on the 70–75° (2θ) area.

Table 1
The lattice parameters and tetragonality ($c(\sqrt{2}a)^{-1}$) of the 2Y-PSZ precursor powders prepared at pH 7 and calcined at various temperatures for 2 h.

Calcination temperature (K)	Lattice parameters (Å)	$c(\sqrt{2}a)^{-1}$
773	$a=3.6143$; $c=5.1503$	1.008
873	$a=3.6061$; $c=5.1437$	1.009
1073	$a=3.6065$; $c=5.1712$	1.014
1273	$a=3.6029$; $c=5.1704$	1.015

The lattice parameters and the tetragonality ($c(\sqrt{2}a)^{-1}$) of the 2Y –PSZ precursor powders prepared pH 7 and calcined at various temperature for 2 h are listed in Table 1. It is seen that the evolution of the tetragonality of the present study was good agreement with the previous result of Viazzi et al. [19].

3.2. Effect of calcination temperatures on the crystallite size and amount of each phase content in 2 Y-PSZ powders

The dependence of the integrated intensity of the predominant reflection peaks and crystallinity on the calcination temperatures of the 2Y-PSZ freeze dried precursor powders is demonstrated in Fig. 5(a) and (b). It reveals that the reflection intensity of t-ZrO_2 phase increases with the calcination temperature increased. But the intensity of $(\bar{1}11)$ reflection peak of m-ZrO_2 phase is no more increased when calcination temperature increased from 773 to 1073 K. This result due to the crystalline amount of t-ZrO_2 increases with the calcination temperature increased, but the m-phase content of ZrO_2 still maintained a low amount level which was no more increased for the same calcination temperature range.

The relationship of the crystallite size of t-ZrO_2, m-ZrO_2 and calcination temperatures is plotted in Fig. 6(a). The crystallite size of t-ZrO_2 increases from 12.3 to 30.2 nm with calcination temperature increased from 773 to 1273 K, whereas the crystallite size of m-ZrO_2 increases from 6.7 to 17.1 nm. In order to determine the activation energy for the crystallite growth of the t-ZrO_2 and m-ZrO_2 obtained in the present study, assume the following equation holds [25].

$$D^n - D_0^n = k\exp\left(-\frac{\Delta E}{RT}\right) \quad (n=2,\ 3) \tag{5}$$

where D is the crystallite size at calcination temperature T for 2 h, D_0 denotes the initial crystallite size before calcination, k is a temperature-independent rate constant, ΔE denotes the activation energy for crystallite growth, R is the gas constant and T denotes the calcination temperature.

When $n=2$, the Eq. (5) is so-called normal crystallite growth equation. Regarding crystallite growth, the crystallite size at T_0 has not been included due to the amorphous

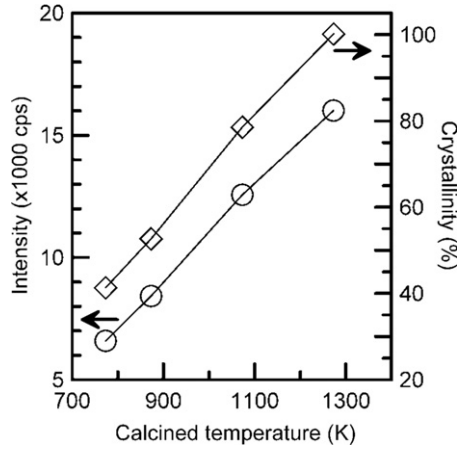

Fig. 5. The dependence of the integrated intensity of the predominant reflection peaks and crystallinity on the calcination temperatures of the 2Y-PSZ freeze dried precursor powders.

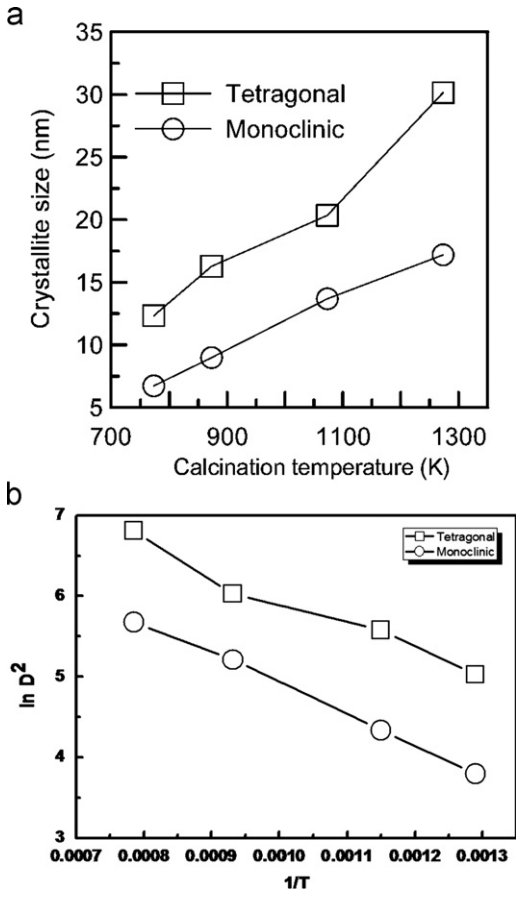

Fig. 6. (a) The effect of calcination temperatures on the crystallite sizes of tetragonal and monoclinic ZrO2 in 2Y-PSZ powders and (b) $\ln D^2$ vs 1/T of t-ZrO_2 and m-ZrO_2.

state of the precursor powders or the sample holding at T_0 is very short. Then the D_0 can be neglected, and Eq. (5) is expressed as

$$D^2 = k\exp\left(-\frac{\Delta E}{RT}\right) \tag{6}$$

$$\ln D^2 = -\frac{\Delta E}{RT} + \ln k \tag{7}$$

Fig. 6(b) shows the plots of the ln D^2 versus 1/T for t-ZrO_2 and m-ZrO_2 crystallites growth when the 2Y-PSZ freeze dried precursor powders as calcined at various temperatures for 2 h, in which the linear relation was obtained. Therefore, calculating the slopes of straight lines in Fig. 6(b), the values of the activation energy (ΔE) for t-ZrO_2 and m-ZrO_2 crystallites growth from the 2Y-PSZ freeze dried precursor powders are obtained, namely, 29.2 and 21.8 kJ/mol, respectively. In the present study, the value of 29.2 kJ/mol is higher than that of 11.50 and 10.48 kJ/mol for both nanosized 8YSZ and 10YSZ [26], and twenty magnitude lower than that of 580 kJ/mol for bulk YSZ [27], but near the 34 kJ/mol of nanosized 2YSZ [28].

According to the results of Figs. 1–4 and used the Eqs. (2) and (3), the amount of t-phase and m-phase of ZrO_2 in 2Y-PSZ powders are obtained. Fig. 7(a) and (b) show the amount of t-phase and m-phase content of ZrO_2, respectively, when the 2Y-PSZ freeze dried precursor powders were calcined at various temperatures for 2 h. It is found that the fraction of m-ZrO_2 was lower than 3.0% when calcination temperatures were lower than 1073 K. But the fraction of m-ZrO_2 rapidly increased to 8.7% with the increase of calcination temperature to 1273 K.

The N_2 absorption/desorption isotherms of 2Y-PSZ freeze dried precursor powders calcined at 873 K for 2 h are shown in Fig. 8(a), it is seen that the curve at a relative pressure (P/P_o) of about 0.4–1.0, has an H_3-type of hysteresis loop because the small particle interconnects created the pores [29]. The BET specific surface area of the 2Y-PSZ freeze dried precursor powders calcinated at 873 K for 2 h is 62.50 m^2/g, which is equivalent to an average particle size of 16.0 nm.

The BET of 2Y-PSZ freeze dried precursor powders calcined at various temperatures for 2 h is shown in Fig. 8(b) which reveals that the BET surface area decreases from 104.2 to 14.4 m^2/g with rising the calcination temperature from 773 K to 1273 K. This result is due to crystallize growth and aggregated increase with rising the calcination temperature leads to the BET surface area decreased. On the other hand, the crystallize sizes determined via XRD and particle sizes determined by BET surface area agree well when calcination temperature lower than 873 K. This result is due to the tetrazonal phase while the monoclinic phase content of ZrO_2 is very small and its size, as determinate, may be omitzed [20]. When the 2Y-PSZ freeze dried precursor powders calcined at 1173 and 1273 K for 2 h, one particle contained about two crystallized tetrazonal ZrO_2. These results also indicate that the powders are virtually nonagglomerated.

The phase transformation from t-ZrO_2 into m-ZrO_2 were occurred when the 2Y-PSZ freeze dried precursor powders calcinations between 873 and 1273 K. However, the fraction of m-ZrO_2 was lower than 1073 K. Moreover, the fraction of m-ZrO_2 rapidly increased to 8.7% with the

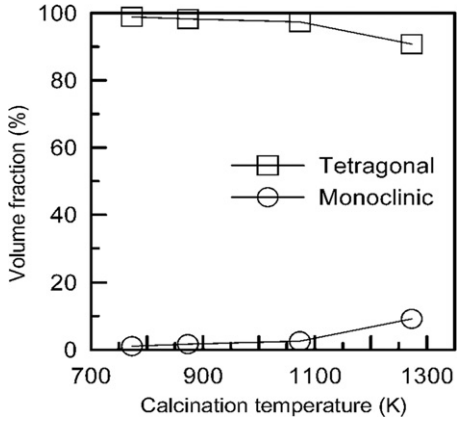

Fig. 7. The volume fraction of tetragonal and monoclinic ZrO_2 content as a function of calcination temperatures in the 2Y-PSZ freeze dried precursor powders.

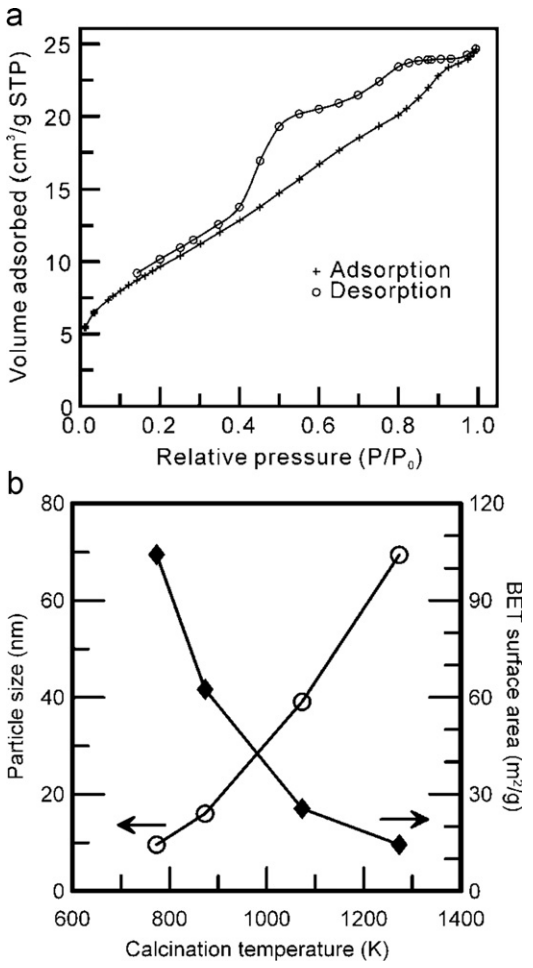

Fig. 8. (a) N_2 absorption/desorption isotherms of 2Y-PSZ freeze-dried precursor powders calcined at 873 K for 2 h and (b) the BET surface area and average particle size as determined by BET for 2Y-PSZ freeze dried precursor powders calcined at various temperature for 2 h.

rising the calcinations temperature to 1273 K. In addition, the crystallite size of t-ZrO_2 was 30.2 nm when calcined at 1273 K for 2 h. However, the crystallite size of m-ZrO_2 was only 17.1 nm. Therefore, the effect of phase transformation of m-ZrO_2 on the BET surface area can be negligible.

3.3. TEM microstructure of 2 Y-PSZ precursor powders calcined at various temperatures for 2 h

Fig. 9 shows the TEM micrographs and selected area electron diffraction (SAED) patterns of the 2Y-PSZ freeze dried precursor powders calcined at 873 K for 2 h. Fig. 9(a) and (b) show the bright field (BF) and dark field (DF) images, respectively, which indicates that the crystallite size was about 26.5 nm, which was in agreement with calculated value from XRD results. The size distribution seems to be uniform. A SAED pattern of the 2Y-PSZ nanocrystallite powders as shown in Fig. 9(c) indicates that the reflections of 101, 103, 104, and 204 from the t-ZrO_2 lattice, and reflections of 102, 222, and 223 from the m-ZrO_2 lattice. The Debye rings indicate that the polycrystalline nature of the powder. When the 2Y-PSZ precursor powders post-calcined at 873 K for 2 h, the crystallinity of ZrO_2 was relatively high, judging from clearly observed lattice image as shown in Fig. 9(d). It indicates that the t-ZrO_2 and m-ZrO_2 coexisting, and presented the $d_{101_t}$and $d_{\bar{1}11_m}$ are 0.297 and 0.313 nm, respectively.

Fig. 10 shows the micrographs, SAED pattern and lattice image of 2Y-PSZ freeze dried precursor powders as calcined at 1273 K for 2 h. Fig. 10(a) and (b) shows the BF and DF images, it indicates that the primary cyrstallites with an average size of 30 nm was mainly aggregated into the secondary aggregates with a mean aggregate particle size of 220.0 nm. Fig. 10(c) and (d) shows the BF and DF images of an aggregate particle with a size of about 116 nm. Fig. 10(e) and (f) shows the SAED patterns of t-ZrO_2 with zone axes (ZA) of $[1\bar{1}0]$ and the m-ZrO_2 with ZA=$[01\bar{2}]$, respectively. Fig. 10(g) shows the lattice image which indicates that d_{101_t}, $d_{\bar{1}11_m}$, d_{110_m} are 0.292, 0.315, and 0.365 nm.

4. Discussion

4.1. The mechanism of ZrO_2 formation

The results of Figs. 1–4 and 6 shows that the m-ZrO_2 content less than 3.0% when the 2Y0-PSZ freeze dried precursor powders calcined at 773–1073 K for 2 h. The absence of the m-ZrO_2 when the first stage is attributed to the close relation between developing t-ZrO_2 and the amorphous reactant or to the small crystallites (11–18 nm) have been reported by Gravie [30], and Mitsuhashi et al. [31]. From the result of Fig. 5, it is found that the size of m-ZrO_2 crystallite is very similar to the co-existing t-ZrO_2 crystallite and never grows to needle like single crystallite. Therefore, one single-domain t-ZrO_2 crystallite must transform instantaneously to one single-domain monoclinic crystallite, in the solid state. The stability of the m-ZrO_2 and t-ZrO_2 forms is believed to depend on crystallite size [30–32].

Since the metastable t-ZrO_2 is known to exist at room temperature only in crystallites of less than ~30 nm diameter, the stability in this case is caused by the lower surface energy of the t-ZrO_2 phase compared with m-ZrO_2 [30]. The surface energy of the m-ZrO_2 ($\gamma_m = 1.13 J/m^2$) [33,34] is higher than that of the t-phase ($\gamma_m = 1.13 J/m^2$) [33,34].

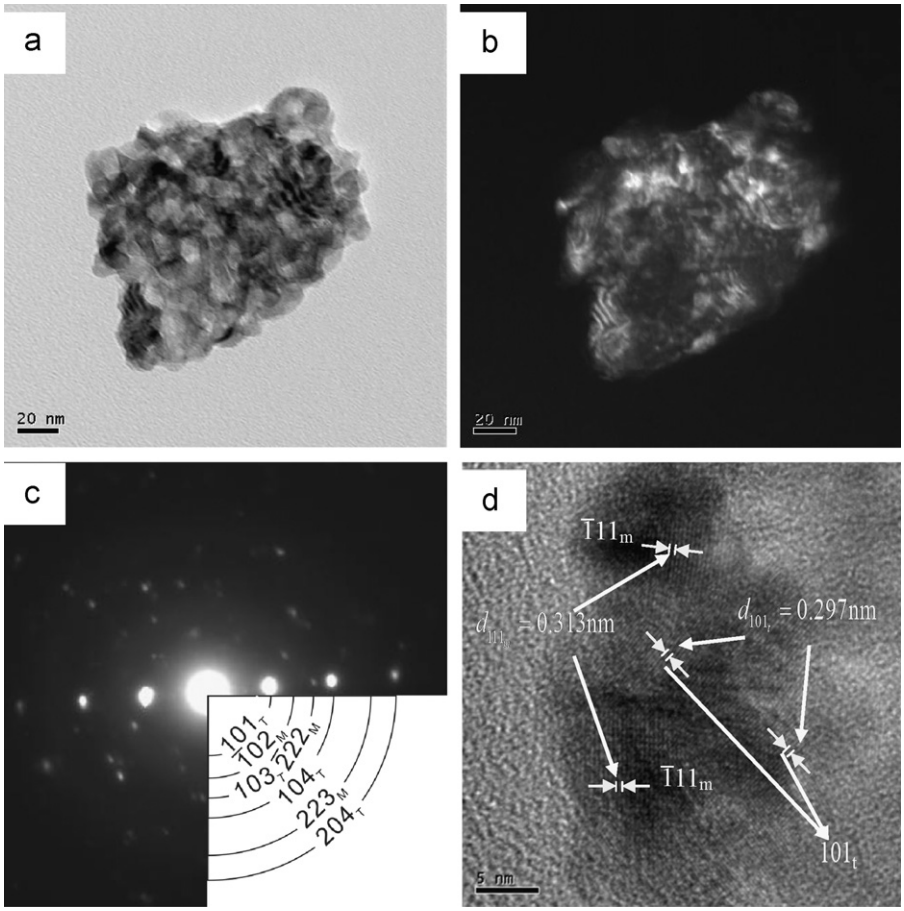

Fig. 9. TEM micrographs of 2Y-PSZ freeze dried precursor powders calcined at 873 K for 2 h: (a) BF image, (b) DF images, (c) SAED pattenis which indexing corresponding to the coexisting of t- and m-ZrO_2 and (d) lattice image showing the d_{101_t} and $d_{\bar{1}11_m}$, respectively.

Wu et al. [15] have pointed out that fraction of the t-ZrO_2 decreases from 52 to 33% when calcination temperature increased from 773 to 973 K for a hold time of 1 h. However, in the present study, the variation trend of the t-ZrO_2 content in 2Y-PSZ powders is not in agreement with the result of Wu et al. [15]. In fact, even at the same holding temperature, growth velocity determined by both transformation activation energy and driving force is different for samples with different crystallite size. Transformation rate depends on activation energy is large and starting temperature for t→m transformation is high when crystallite size is large, which leads to a large growth velocity. When the crystallite size is small, although incubation period is short, the transformation rate thereafter is small, which results in large volume fraction of isothermal m-phase produced. Therefore, the incubation period is determined by critical nucleation energy barrier and densities of nucleation sites; transformation rate depends on activation energy for transformation [14].

4.2. The growth mechanism of t- and m- ZrO_2 from the 2Y-PSZ freeze dried precursor powders

TEM microstructure of the coarse-crystallite specimen is shown in Figs. 9 and 10 which reveals the coexistence of t- and m-ZrO_2 dual phase in the same crystallite due to the m-ZrO_2 nucleate preferentially at the interface of the crystallites and grow inward across the crystallite when they impeded by growing m-ZrO_2 crystallite from the opposite direction and thus terminate inside the original t-ZrO_2 crystallite have been reported by Zhu and Yan [14]. Moreover, from Figs. 8 and 9 it is also found that the crystallites exist in the forms of either t-ZrO_2 or t-plus m-ZrO_2 rather than solely m-ZrO_2 [13]. Hanlyn-Harris and St. John [35] pointed out that exists a critical diameter (dc) for a certain type of Y_2O_3–ZrO_2 ceramic and during the crystallite size of t-phase is larger than dc, then, t→m transformation will occur and microstructure of the crystallite will consist of m-phase. Otherwise, the crystallite will be in the form of t-phase.

By the formation model of metastable phase in the solid state [35], change in m-ZrO_2 crystallite size and morphology may involve a combination of three processes: (1) m-ZrO_2 and t-ZrO_2 crystallites attach in an oriented way and m-ZrO_2 crystallite coarsens by transformation from t-ZrO_2 crystallites; (2) m-ZrO_2 sandwiched by oriented t-ZrO_2 crystallites is partly (and ultimately, completely) consumed by conversion to t-ZrO_2 and (3) m-ZrO_2 forms at t-ZrO_2 twin surface. Surface energy can significantly modify phase relationships when the crystallite size is very small.

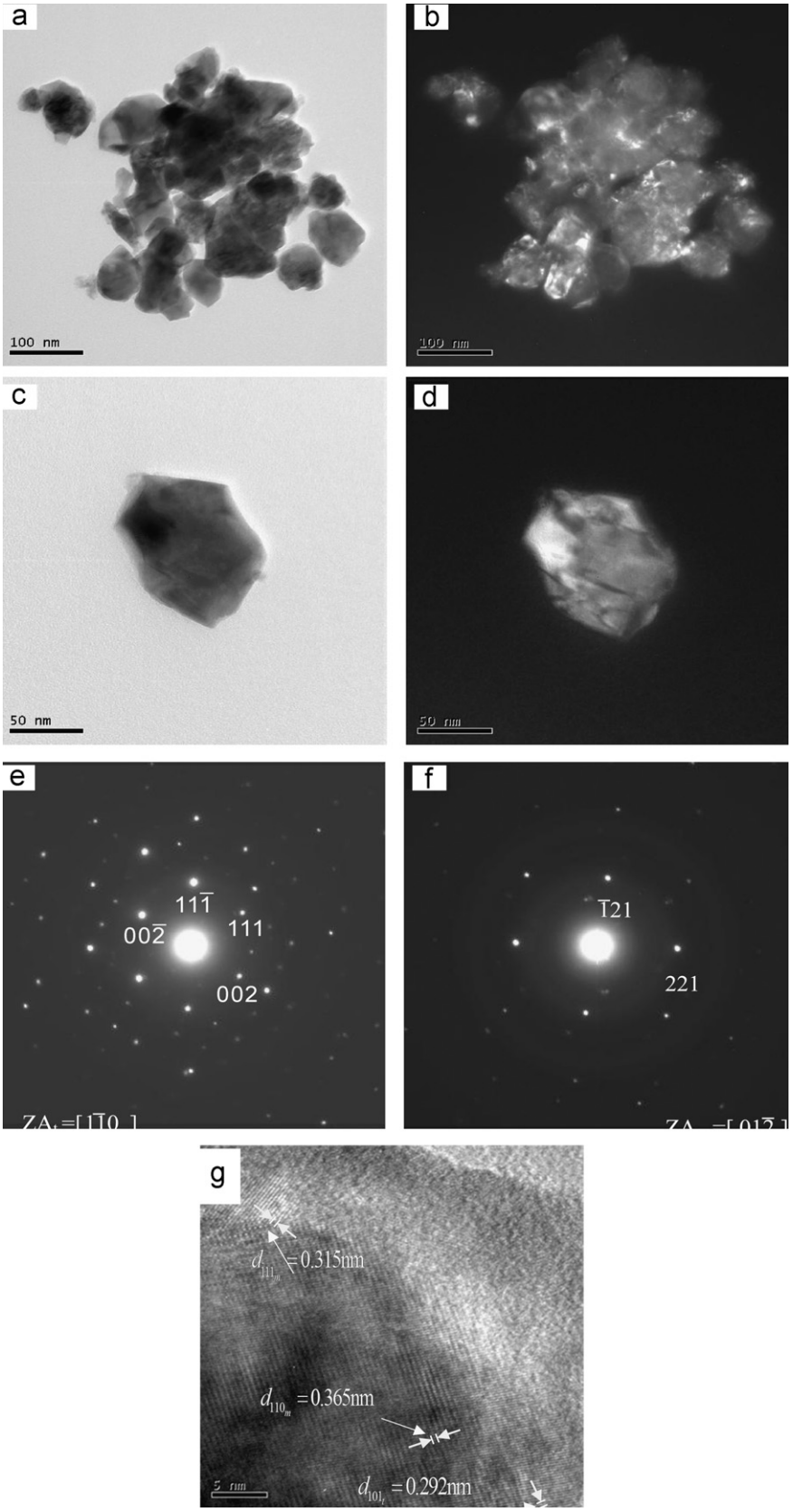

Fig. 10. TEM micrographs of the 2Y-PSZ freeze dried precursor powders as calcined at 1273 K for 2 h: (a) BF image, (b) DF image, (c) BF image of aggregate particle, (d) DF image of aggregate particle (e), (f) SAED pattern which indexing corresponding to the t-ZrO_2 with ZA=[1$\bar{1}$0] and m-ZrO_2 with ZA=[01$\bar{2}$], respectively, and (g) lattice image indicating d_{101t}, $d_{\bar{1}11m}$ and d_{110m}.

An important conclusion from this study is the general result that oriented attachment and growth can lead to formation of planar defects, including stack faults and other interfaces. These microstructures are direct consequence of a coarsening mechanism that involves surface tension reduction by elimination the attachment surface that is constrained only in the two dimensions of the interface [36].

In the present study, the activation energy of t-ZrO_2 crystallite growth is only 29.2 kJ/mol. Chen et al. [28] pointed out that using mixed 0.1 M $ZrOCl_2 \cdot 8H_2O$ and YCl_3 precursor solution under the processing conditions of pH 9.5 and 2 wt% polyglycol (MWpeg = 2000 g/mol), the activation energy of crystallite growth about 34.03 kJ/mol was obtained for the 2Y-PSZ powder within the calcination temperature range of 873–1273 K. This value is much lower than that observed for the about 580 kJ/mol of bulk YSZ [27]. Similar result has also been reported for other ceramics, namely ZnO [37], where the growth activation energy in the nanocrystallite is observed to be about 20 kJ/mol, while that for microcrystalline grains are observed to be about 275 kJ/mol. Moreover, this result accords well with the activation energy (~32–44 kJ/mol) of nano SnO_2 growth [38], and this fact is further confirmed by the experimental result of activation energy about 40 kJ/mol for pure nano ZrO_2 growth [39]. It is obvious that the very slow activation energy of crystallite growth appears to be a characteristic feature of nano crystalline oxide ceramics.

When a low-valence cation dopant, such as Y^{3+}, it is introduced into the ZrO_2 lattice, oxygen vacancies are created to maintain local electrical neutrality [40]. Due to the large size of Y^{3+} cations relative to Zr^{4+} cations, the generated oxygen vacancies tend to be associated with Zr^{4+} cations [41], which reduce the effective coordination number of Zr^{4+} cations below 7. Moreover, the crystal chemistry model also postulates that the dopant Y^{3+} cations would also favor this eight-fold coordination with oxygen [42]. Therefore, these effects are reflected in the stabilization of the tetragonal phase in 2Y-PSZ [28]. On the other hand, the presence of large number of oxygen vacancies on grain surface, which mainly comes from the doping of Y^{3+} [43] and nano-size effect [44], which makes the surface energy increase drastically and decrease the growth activation energy of nanoparticles [28].

5. Conclusions

The phase transformation and crystallite growth behavior of 2 mol% ytttia-partially stabilized zirconia (2Y-PSZ) freeze dried precursor powders have been investigated using X-ray diffraction (XRD), Brunauer–Emmett–Teller (BET) isotherm, transmission electron microscopy (TEM) and selected area electron diffraction (SAED). When the 2Y –PSZ freeze dried precursor powders was calcined at 773 to 1273 K for 2 h, the XRD results show that the crystallized phases to be composed of the major phase tetragonal-ZrO_2 (t-ZrO_2) and a minor phase of monoclinic- ZrO_2 (m-ZrO_2). The volume fraction of m-ZrO_2 content is maintained at about 3.0% when the 2Y-PSZ freeze dried precursor powder calcination was lower than 1073 K. Whereas, the volume fraction of the m-ZrO_2 rapidly increases from 3.0 to 8.7% with rising the calcination temperature from 1073 to 1273 K. The crystallite sizes of t- and m- ZrO_2 increase from 12.3 to 30.2 nm and 6.7 to 17.1 nm, respectively, with rising the calcination temperature from 773 to 1273 K. In addition, the activation energies of crystallites growth for t- and m-ZrO_2 in the 2Y-PSZ freeze dried precursor powders are 29.2 and 21.8 kJ/mol, respectively. When the 2Y-PSZ freeze dried precursor powders are calcined at 1273 K for 2 h, the microstructure of TEM shows that the primary crystallites with an average size about of 30.0 nm was mainly aggregated into the secondary with a mean aggregate particle size of 220.0 nm.

Acknowledgment

The authors gratefully acknowledge the support of the Ministry of Economic Affairs, Taiwan, Republic of China, under Grant 101-EC-17-A-08-S1-142 and National science council, Taiwan (NSC95-2221-E-037-007), and Prof. M. H. Hon for discussion in the manuscript preparation and Mr. S. Y. Yau for TEM photography.

References

[1] C. Piconi, G. Maccauro, Zirconia as a ceramic biomaterial, Journal of the European Ceramic Society 20 (1999) 1–25.
[2] J.R. Kelly, Ceramics in restorative and prosthetic dentistry, Annual Review of Materials Science 27 (1997) 443–468.
[3] K.H. Meyenberg, H. Lűthy, D. Schärer, Zirconium posts. A new all-ceramic concept for nonvital abutment teeth, The European Journal of Esthetic Dentistry 7 (1995) 73–80.
[4] A. Wohlwend, S. Studer, P. Schärer, The zirconium oxide abutment: an all-ceramic abutment for the esthetic improvement of implant superstructures quintessence, Journal of Dental Technology 1 (1997) 63–74.
[5] T. Kosmača, Č. Oblakb, L. Marion, The effects of dental grinding and sandblasting on ageing and fatigue behavior of dental zirconia (Y-TZP) ceramics, Journal of the European Ceramic Society 28 (2008) 1085–1090.
[6] I. Denry, J.R. Kelly, State of the art of zirconia for dental application, Journal of Dental Materials 24 (2008) 297–307.
[7] E.C. Subbarao, in: A.H. Heuer, L.W. Hobbs (Eds.), In Advances in Ceramics, Vol. 3, The American Ceramic Society, Columbus, OH, 1981, p. 1.
[8] C. Pascual, P. Duran, Subsolidus phase equilibria and ordering in the system ZrO2–Y_2O_3, Journal of the American Creamic Society 66 (1983) 23–27.
[9] A.H. Heuer, Transformation toughening in ZrO_2-containing ceramics, Journal of the American Creamic Society 70 (1987) 689–698.
[10] F.F. Lange, Transformation toughening. Part 4. Fabrication, fracture-toughness and strength of Al_2O_3–ZrO_2 composites, The Journal of Materials Science 17 (1982) 247–252.
[11] F.F. Lange, Transformation toughening. Part 5. Effect of temperature and alloy on fracture toughness, The Journal of Materials Science 17 (1982) 255–262.
[12] S. Deville, J. Chevalier, G. Fantozzi, J.F. Bartolomé, J. Requena, J.S. Moya, R. Torrecillas, L.A. Díaz, Low-temperature aging of zirconia-toughened alumina ceramics and its implication in biomedical implants, Journal of the American Creamic Society 23 (2003) 2975–2982.

[13] M.R. Álvarez, A.R. Landa, L.C. Otero-Dìaz, M.J. Torralvo, Structural and textural study on ZrO_2–Y_2O_3 powders, Journal of the American Creamic Society 18 (1998) 1201–1210.
[14] W.Z. Zhu, M. Yan, Effect of grain size on the kinetics of isothermal tetragonal to monoclinic transformation in ZrO_2 (2 mol% Y_2O_3) ceramics, Journal of the American Creamic Society 17 (1997) 1729–1739.
[15] N.L. Wu, T.E. Wu, Enhanced phase stability for tetragonal zirconia in precipitation synthesis, Journal of the American Creamic Society 83 (2000) 3225–3227.
[16] O. Vasylkiv, Y. Sakka, Synthesis and colloidal processing of zirconia nanopowder, Journal of the American Creamic Society 84 (2001) 2489–2494.
[17] W. Li, L. Gao, Nano $ZrO_2(Y_2O_3)$ particles processing by heating of ethanol-aqueous salt solutions, Ceramics International 27 (2001) 543–546.
[18] W. Li, W.L. Gao, Compacting and sintering behavior for nano ZrO_2 powders, Scripta Materialia 44 (2001) 2267–2272.
[19] C. Viazzi, J.P. Bonino, F. Ansart, A. Barnabé, Structural study of metastable tetragonal YSZ powders produced via a sol–gel route, The Journal of Alloys and Compounds 452 (2008) 377–383.
[20] C.W. Kuo, Y.H. Shen, S.B. Wen, H.E. Lee, I.M. Hung, M.C. Wang, Phase transformation kinetics of 3 mol% yttria partially stabilized zirconia (3Y-PSZ) nanopowders prepared by a non-isothermal process, Ceramics International 37 (2011) 341–347.
[21] Y.W. Hsu, K.H. Yang, K.M. Chang, S.W. Yeh, M.C. Wang, Synthesis and crystallization behavior of 3 mol% yttria stabilized tetragonal zirconia polycrystals (3Y-TZP) nanosized powders prepared using a simple co-precipization process, The Journal of Alloys and Compounds 509 (2011) 6864–6870.
[22] B.D. Cullity, Elements of X-ray Diffraction, Addison-Wesley, Reading, MA, 1967 388.
[23] R.C. Garvie, P.S. Nicholson, Phase analysis in zirconia system, Journal of the American Ceramic Society 55 (1972) 303–305.
[24] Q. Zhu, B. Fan, Low temperature sintering of 8YSZ electrolyte film for intermediate temperature solid oxide fuel cells, Solid State Ionics 176 (2005) 889–894.
[25] S.L. Hwang, I.W. Chen, Grain size control of tetragonal ziconia polycrystals using the space change concept, Journal of the American Ceramic Society 73 (1990) 3269–3277.
[26] C.W. Kuo, Y.H. Shen, I.M. Hung, S.B. Wen, H.E. Lee, M.C. Wang, Effect of Y_2O_3 addition on the crystal growth and sintering behavior of YSZ nanopowders prepared by a sol–gel process, The Journal of Alloys and Compounds 472 (2009) 186–193.
[27] T.G. Neigh, J. Wadsworth, Superelastic behaviou of a fine-grained, yttria-stabilized, tetragonal zirconia polycrystal, Acta Metallurgica et Materialia 38 (1990) 1121–1133.
[28] S.G. Chen, Y.S. Yin, D.P. Wang, J. Li, Reduced activation energy and crystalline size for yttria stabilized zirconia nano-crystals: an experimental and theoretical study, Journal of Crystal Growth 267 (2004) 100–109.
[29] G. Ertl, H. Knozinger, J. Weithamp, Handbook of Heterozeneous Catalysis. WCHD, 6945, Weinheim, Vol. 3 (1997), p. 1508.
[30] R.C. Gravie, Occurrence of metastable tetragonal zirconia as a crystallite size effect, The Journal of Physical Chemistry 69 (1965) 1238–1243.
[31] T. Mitsuhashi, M. Ichihara, U. Tatsuke, Characterization and stabilization of metastable tetragonal ZrO_2, Journal of the American Ceramic Society 57 (1974) 97–101.
[32] H.J. Huang, M.C. Wang, The phase formation and stability of tetragonal ZrO_2 prepared in a silica bath, Ceramics International 39 (2013) 1729–1739.
[33] I.W. Chen, R.J. Chiao, Martensitic nucleation in ZrO_2, Acta Metallurgica 31 (1983) 1627–1638.
[34] T. Chraska, A.H. King, C.C. Berndt, On the size-dependent phase transformation in nanoparticulate zirconia, Materials Science and Engineering: A A206 (2000) 169–178.
[35] J.H. Hanlyn-Harris, D.H. John St, An investigation of ternary Mg–Ce-PSZ, Materials Science Forun 34-36 (1988) 141–145.
[36] R.L. Penn, J.F. Banfield, Oriented attachment and growth, twing, polytypism, and formation of metastable phase: Insights from nanocrystalline TiO_2, American Mineralogist 83 (1998) 1077–1082.
[37] A.P. Hynes, R.H. Doremus, R.W. Siegel, Sintering and characterization of nanophase zinc oxide, Journal of the American Ceramic Society 85 (2002) 1979–1987.
[38] J.K.L. Lai, C.H. Shek, G.M. Lim, Grain growth kinetics of nanocrystalline SnO_2 for long-term isothermal annealing, Scripta Materialia 49 (2003) 441–446.
[39] G. Baldinozzi, D. Simeone, D. Gosset, M. Dutheil, Neutron diffraction study of the size-induced tetragonal to monoclinic phase transition in zirconia nanocrystals, Physical Review Letters 90 (2003) 216103-1–216103-4.
[40] M. Hillert, Thermodynamic model of the cubic tetragonal transition in nonstocichiometric zicronia, Journal of the American Creamic Society 74 (1991) 2005–2006.
[41] A. Bogicevic, C. Wolverton, G.M. Crosbie, E.B. Stechel, Defect ordering in aliovalently doped cubic zirconia from first principles, Physical Review B 64 (2001) 014106-1–014106-14.
[42] S.M. Ho, On the structural chemistry of zirconium oxide, Materials Science and Engineering: A 54 (1982) 23–29.
[43] S. Shukla, S. Seal, R. Vij, S. Bandyopadhyay, Reduced activation energy for grain growth in nanocrystalline yttria-stabilized zirconia, Nano Letters 3 (2003) 397–401.
[44] X.D. Zhou, W. Huebner, Size-induced lattice relaxation in CeO_2 nanoparticles, Applied Physics Letters 79 (2001) 3512–3514.